Atmos. Meas. Tech. Discuss., 8, 6355–6393, 2015
www.atmos-meas-tech-discuss.net/8/6355/2015/
doi:10.5194/amtd-8-6355-2015


Atmospheric Measurement Techniques Discussions



# Measurement of non-volatile particle number size distribution

**G. I. Gkatzelis**[1,2], **D. K. Papanastasiou**[1,2], **K. Florou**[1,2], **C. Kaltsonoudis**[1,2], **E. Louvaris**[1,2], **and S. N. Pandis**[1,2,3]

[1]Institute of Chemical Engineering Sciences, ICE-HT, Patras, Greece
[2]Department of Chemical Engineering, University of Patras, Greece
[3]Department of Chemical Engineering, Carnegie Mellon University, Pittsburgh, USA

Received: 30 March 2015 – Accepted: 21 May 2015 – Published: 25 June 2015

Correspondence to: S. N. Pandis (spyros@chemeng.upatras.gr)

Published by Copernicus Publications on behalf of the European Geosciences Union.







## Abstract

An experimental methodology was developed to measure the non-volatile particle number concentration using a thermodenuder (TD). The TD was coupled with a high-resolution time-of-flight aerosol mass spectrometer, measuring the chemical composition and mass size distribution of the submicrometer aerosol and a scanning mobility particle sizer (SMPS) that provided the number size distribution of the aerosol in the range from 10 to 500 nm. The method was evaluated with a set of smog chamber experiments and achieved almost complete evaporation (> 98 %) of secondary organic as well as freshly nucleated particles, using a TD temperature of 400 °C and a centerline residence time of 15 s.

This experimental approach was applied in a winter field campaign in Athens and provided a direct measurement of number concentration and size distribution for particles emitted from major pollution sources. During periods in which the contribution of biomass burning sources was dominant, more than 80 % of particle number concentration remained after passing through the thermodenuder, suggesting that nearly all biomass burning particles had a non-volatile core. These remaining particles consisted mostly of black carbon (60 % mass contribution) and organic aerosol, OA (40 %). Organics that had not evaporated through the TD were mostly biomass burning OA (BBOA) and oxygenated OA (OOA) as determined from AMS source apportionment analysis. For periods during which traffic contribution was dominant 50–60 % of the particles had a non-volatile core while the rest evaporated at 400 °C. The remaining particle mass consisted mostly of black carbon (BC) with an 80 % contribution, while OA was responsible for another 15–20 %. Organics were mostly hydrocarbon-like OA (HOA) and OOA. These results suggest that even at 400 °C some fraction of the OA does not evaporate from particles emitted from common combustion processes, such as biomass burning and car engines, indicating that a fraction of this type of OA is of extremely low volatility.





AMTD
8, 6355–6393, 2015



## 1 Introduction

Atmospheric aerosols, also known as particulate matter (PM), are defined as a suspension of fine solid or liquid particles in a gaseous medium. These particles range in size from a few nanometers in diameter to as much as 100 µm. Aerosols consist of inorganic ions, organic compounds, oxides of most metals, elemental carbon, and water with organic compounds often being the dominant fraction of submicrometer PM, with a contribution of 20–90 % depending on the location site (Kanakidou et al., 2005).

Fine particles ($PM_{2.5}$) can affect human health by penetrating into the respiratory tract, and reaching deep into the lungs (Miller et al., 1979; Dockery et al., 1993; Künzli et al., 2005; Wyler et al., 2000; Cohen et al., 2005). Toxicological data suggests that ultrafine particles whose diameter is < 100 nm, can have adverse pulmonary and cardiovascular effects (Donaldson and MacNee, 2001). Ultrafine particles soluble in water and lipids have a minor contribution to the total aerosol mass and are believed to have minor effects on human health (Kreyling and Scheuch, 2000) but insoluble components, like black carbon (BC), could have more significant health impacts. The impacts of these insoluble particles cannot be easily determined with mass measurements but require studies of the number concentration.

Atmospheric particulate matter can also affect the Earth's radiative budget and global climate. Particles act as cloud condensation nuclei, form cloud droplets and scatter light, leading to cooling of the planet. Absorbing aerosol components, such as black carbon (BC), contribute to warming by strongly absorbing light. BC containing particles, mostly emitted by combustion sources evolve due to coagulation or condensation of vapors (Scheer et al., 2005). This coating of BC particles can increase their light absorption up to a factor of three (Andreae and Gelencsér, 2006; Saleh et al., 2014) but also their hygroscopicity (Kuwata et al., 2008). The number concentration, size distribution and mixing state of BC particles is essential in understanding their effect on climate (Bond et al., 2013).





AMTD
8, 6355–6393, 2015



Since the number concentration of ultrafine atmospheric particles, especially of the nonvolatile BC particles, plays a key role in both their health and climate effects, ways to measure these particles have been proposed. Nonvolatile particles have been indirectly measured by heating up the aerosol through thermodenuders. TDs (Wehner et al., 2002; Burtscher et al., 2001), have been used to quantify the volatility of particles at low and intermediate temperatures (An et al., 2007; Kim et al., 2010) but also their nonvolatile fraction at higher temperatures (> 250 °C). Wehner et al. (2004) suggested that by heating up the particles at 280 °C for residence times up to 9 s, sulfates, nitrates and most organics evaporate and only non-volatile particles and cores remain. To measure the number particle size distribution in this size range scanning mobility particle sizers (SMPS) have been used after the TD (Wehner et al., 2004; Kim et al., 2010; Saleh et al., 2012). For the determination of the chemical composition of these particles aerosol mass spectrometers (AMS) have been increasingly applied (Lee et al., 2010; Poulain et al., 2010; Cappa and Jimenez, 2010).

Despite the increasing focus on non volatile particles their contribution to the total number size distribution remains uncertain and strongly depends on the different pollution sources. Chemical characterization of these non volatile particles can provide insights about their chemical composition, information about the contribution of BC to the total number concentration and improve the characterization of different emission sources.

In this work an experimental methodology is developed and evaluated to measure the non-volatile particle number concentration. The method was tested with a set of chamber experiments to investigate its ability to evaporate particles formed from traditional biogenic and anthropogenic SOA precursors and most important, particles coming from a nucleation event. This experimental approach was applied during the Athens-2013 winter campaign to examine the number concentration of nonvolatile particles in an urban environment, their chemical composition and size distribution as well as the contribution of different pollution sources.





AMTD
8, 6355–6393, 2015



## 2 Thermodenuder-description

The TD setup used in this study was based on the design of An et al. (2007). A detailed schematic of the TD apparatus is shown in Fig. 1. The TD consists of the bypass (BP) line, which operates at ambient temperature and the TD line, which was set at 400 °C in this study. Automatically operated three-way valves placed on the aerosol inlet and outlet (Fig. 1), allow rapid switching between the BP and TD lines and a comparison of the two, essential for particle evaporation and volatility measurements. The TD line includes two main parts: (i) the TD heating section and (ii) the TD cooling section. The TD heating section has a length of 0.5 m and an inner diameter of 36.4 mm. Fine sand is used to cover the inner stainless steel tube to avoid temperature fluctuations. A PID controller (model CNi, I/32, Omega) controls the TD temperature through a heating tape wrapped around the outer cylinder (diameter = 100 mm) of the TD, based on readings of a thermocouple (TJ36 Series, Omega) placed in the center of the heating tube. The heating section is insulated to minimize losses to the surroundings. The cooling section has the same dimensions as the heating section and consists of a cylindrical stainless steel gauze with an inner diameter of 36.4 mm. The stainless steel gauze is covered with an activated carbon jacket which is used to remove organic and inorganic vapors that evaporated from the particle phase avoiding thus re-condensation during the cooling stage.

The residence time inside the TD has been shown to be a critical parameter for particle evaporation (Riipinen et al., 2010). In this study, a flow rate of 1 L $min^{-1}$ inside the TD line was used. The flow in the system is laminar and results in different residence times, based on radial position. The centerline travel time of the particles was 15 s, significantly longer than most commercial and research TDs.

The temperature profile of the TD when set at 400 °C, is shown in Fig. 2. The temperature profile was measured by a stainless steel thermocouple (50 cm length, Omega) in the center of the TD tube. The temperature difference between the center of the TD tube and the walls was less than 10 °C. The walls of the TD were warm even before the





AMTD
8, 6355–6393, 2015



heating section, due to conduction, resulting in pre-heating of the particles before entering the heating tube. The aerosol sample already has a temperature of 150 °C when introduced in the heating section, which increases to the set temperature of 400 °C after 7 s, 20 cm from the TD inlet. Particles remain at the set temperature of 400 °C for more than 7 s. Similar results were reported by Wehner et al. (2002) using a similar TD setup.

### 2.1 Particle wall losses

Aerosol losses inside the TD at 400 °C were determined in a separate set of experiments, using NaCl particles, since their evaporation is negligible even at high temperatures (Burtscher et al., 2001). NaCl aerosol was produced by atomizing (constant output atomizer, aerosol generator 3076, TSI) aqueous NaCl solutions of known concentrations in the range between 0.5 and 3 g $L^{-1}$ (NaCl purity ≥ 99.5 %, Sigma). The produced NaCl droplets flowed through a silica dryer (RH < 20 %) and then the dry particles passed through the TD. Particles exiting the TD were measured with a scanning mobility particle sizer (SMPS, TSI Classifier model 3080, TSI DMA 3081, TSI Water CPC 3787) which operated with sheath and sample air flows set at 5 and 1 L $min^{-1}$ respectively. The aerosol number size distribution (10 to 500 nm) was measured every 3 min (SMPS scanning time). Sampling both the TD and the BP line was achieved by automatic switching (every 3 min, synchronized with the SMPS) of the 3-way valves (Fig. 1). Experiments were conducted in a wide range of particle mass and number concentrations ranging from 50 to 300 µg $m^{-3}$ and $10^4$ to $10^5$ $cm^{-3}$, respectively. Particle wall loss inside the TD line was determined relative to the BP line using:

$$\text{Loss}\,(D_\text{p}) = \frac{[\text{d}N/\text{d}\log D_\text{p}]_\text{TD}}{[\text{d}N/\text{d}\log D_\text{p}]_\text{BP}}, \quad (1)$$

where $\text{d}N/\text{d}\log D_\text{p}$ is the number concentration for the TD and BP measurements and $D_\text{p}$ is the mobility diameter of the particles.





AMTD
8, 6355–6393, 2015



Particle wall loss was determined at 400 °C and the average result from all 9 experiments is given in Fig. 3. The results indicate that up to 70 % of the particles smaller than 30 nm, are lost on the walls while for particles larger than 50 nm the losses are around 50 %. Small particles are lost to the walls mostly due to Brownian diffusion, while for larger particles, thermophoretic losses prevail (Burtscher et al., 2001). The precision of the measurements ($\pm 2\,\sigma$) for particles smaller than 100 nm is < 10 % while for larger particles increases up to around 20 %. The focus of this work is on particles smaller than 100 nm so the corresponding losses have been determined quite precisely.

The average particle wall loss function determined, was fitted with a triple-exponential function.

$$(\%)\,\mathrm{Loss}\,(D_\mathrm{p}) = 1.28\exp(-0.1\cdot D_\mathrm{p}) + 0.47\exp(2\times 10^{-4}\cdot D_\mathrm{p}) - 0.64\exp(-0.11\cdot D_\mathrm{p}) \quad (2)$$

The resulting fit parameters (Fig. 3) were used to correct all the measurements throughout this work.

## 3 Thermodenuder characterization

### 3.1 Evaporation of SOA

The TD methodology was tested in a set of laboratory experiments performed using the indoor smog chamber facility at ICE-HT/FORTH, Patras. The chamber is a 10 $m^3$ Teflon reactor suspended in a temperature controlled room (~ 30 $m^3$) with aluminum coated walls. The room walls are covered with UV/Vis lamps (320–450 nm wavelength range). The photolytic rate of $NO_2$ was measured using the well-established chemical actinometry method (Bohn et al., 2005), giving a $J_{NO_2} = 0.59\,\mathrm{min}^{-1}$. In all experiments the temperature and the RH inside the chamber were kept constant at 25 °C and < 30 %, respectively.

Volatile organic compounds (VOCs) were measured using a proton transfer mass spectrometer (PTR-MS, Ionicon)(de Gouw and Warneke, 2007), and $O_3$ and $NO_x$ were





AMTD
8, 6355–6393, 2015



measured with the corresponding online monitors (Model 400E Photometric Ozone Analyzer, Teledyne and Model T200 Nitrogen Oxide Analayzer, Teledyne). The TD was coupled with a high-resolution time-of-flight aerosol mass spectrometer (HR-ToF-AMS, Aerodyne) measuring the chemical composition and mass size distribution of the submicrometer aerosol. A scanning mobility particle sizer (SMPS, TSI) connected to the TD provided the number size distribution of the aerosol in the diameter range from 10 to 500 nm. The SMPS was operated with sheath and sample air flows set at 5 and 1 L $min^{-1}$, respectively. The AMS and SMPS were synchronized to measure, either from the BP line (ambient conditions) or the TD line (400 °C) every 3 min.

### 3.1.1 Biogenic SOA

For the generation of biogenic SOA a set of experiments utilizing the dark ozonolysis of $\alpha$-pinene were conducted following the experimental conditions given by Pathak et al. (2007), shown in Table 1. First, $O_3$ was introduced inside the chamber and then an injection of $\alpha$-pinene initiated the production of SOA. The experiment took place at $NO_x$ mixing ratio < 2 ppb in the absence of particle seeds. The SOA mass concentration was determined from the measured SMPS size distribution using a density of 1.4 g $cm^{-3}$ (Kostenidou et al., 2007).

Time series for particle number distribution of SOA particles formed from $\alpha$-pinene ozonolysis at ambient temperature (BP) and 400 °C (TD) for experiment 1 (Table 1) is shown in Fig. 4. After the introduction of $O_3$ at 00:45 and injection of $\alpha$-pinene at 01:20, new particles were formed and grew rapidly up to 100 nm in less than one hour, reaching a concentration of around 2000 $cm^{-3}$. These fresh SOA particles evaporated almost completely (2 % remained) after passing through the TD line at 400 °C (Fig. 4).

The particle number size distribution in the chamber at the end of the experiment is shown in Fig. 5. A significant decrease of total particle number concentration, from 1700 to 35 $cm^{-3}$ (number fraction remaining ~ 2.2 %), after sampling through the TD line was observed. After new particle formation occurred the number fraction remaining (NFR) immediately dropped to 2 % showing a 98 % particle evaporation in the TD line.





AMTD
8, 6355–6393, 2015



This shows that fresh SOA formed from $\alpha$-pinene ozonolysis evaporates almost completely after heated at 400 °C. The few remaining particles after the TD were mainly preexisting particles in the chamber. Background particle number concentration after the TD was around 20 $cm^{-3}$ before the reactions started and this value was relatively stable during the experiment.

### 3.1.2 Anthropogenic SOA

As a typical example of anthropogenic SOA, the photooxidation of toluene was examined to test the ability of the proposed TD methodology to completely evaporate anthropogenic SOA. $H_2O_2$ and toluene were injected in the chamber and after reactants were mixed, the UV lights were turned on, initiating the photochemistry. OH radicals were produced from $H_2O_2$ photolysis and OH concentration inside the chamber was determined following the decay of toluene. The experiments were conducted at $NO_x$ mixing ratio of < 10 ppb in the absence of particle seeds. A summary of the experimental conditions is given in Table 1.

The time evolution of the number size distribution of experiment 1 is shown in Fig. 6. After injecting toluene and $H_2O_2$ at 00:30, UV lights were turned on (00:45), forming fresh particles at 25 °C. The growth of these particles up to 100 nm took place in less than one hour reaching a concentration of 1300 $cm^{-3}$. When heated at 400 °C these fresh particles evaporated practically completely (2 to 4 % remained).

The average number size distributions from 07:00 to 09:00 are shown in Fig. 7. Again, a significant decrease of the particle number concentration was observed from 1350 to 60 $cm^{-3}$ (NFR = 4 %). After new particle formation NFR was less than 5 % and as particle number concentration increased NFR decreased to 2 % suggesting that 98 % of the particles evaporated at 400 °C. Background particle number concentration after the TD was around 30 $cm^{-3}$ before the reactions started and increased during the experiment to 70 $cm^{-3}$ suggesting that a small fraction of the newly formed particles did not evaporate through the TD (1–2 %). This shows that fresh SOA particles formed from toluene photooxidation evaporate almost completely after heating at 400 °C.





AMTD
8, 6355–6393, 2015



### 3.2 Evaporation of freshly nucleated particles

Furthermore, a set of measurements was conducted to explore the ability of this technique to evaporate freshly nucleated particles that originate from photoxidation of ambient air mixtures enclosed in a chamber.

Experiments were performed in a 10 $m^3$ Teflon chamber, while OH radicals were generated from $H_2O_2$ photolysis ($J_{NO_2} \sim 0.59\,min^{-1}$). Ambient air present in typical summer days in Patras (Kostenidou et al., 2015) was introduced inside the chamber and characterized under dark conditions with the full suite of instruments as given in Table 2. After the initial characterization, the ambient air was exposed to UV light, initiating OH photochemistry. Typical [OH] ranged from $3.1–4.2 \times 10^6$ molecules $cm^{-3}$, as determined by the decay of a suitable tracer (n-butanol, d9) detected by PTR-MS (Barmet et al., 2012).

The time series for particle number size distribution for a typical experiment is shown in Fig. 8. After the chamber background measurement (phase A), ambient air is introduced inside the chamber and characterized (phase B). In most experiments the initial total particle number ranged from 300–500 $cm^{-3}$, about half of what is measured in the atmosphere outside the chamber facility during the chamber filling stage, mostly due to dilution and losses through the transfer setup. Particulate mass ($PM_1$) ranged from 2 to 5 $\mu g\,m^{-3}$ and as determined from AMS its chemical composition was organics (55 %), sulfate (30 %), ammonium (10 %) and nitrate (5 %), while its O : C ratio was about 0.6. A large fraction (40–45 %) of these aged particles seem to be persistent at 400 °C as can been seen in Fig. 9, indicating their extremely low volatility nature.

During phase C, and after the initiation of photochemistry, significant new particle formation occurred ($\sim 4000\,cm^{-3}$ new particles formed), followed by phase D, where significant particle growth was observed. AMS measurements showed that these new particles mainly consisted of organics of low enough volatility to nucleate, however a small contribution of particulate sulfate and ammonium cannot be excluded. Figure 10 shows the number size distributions a little after the nucleation event occurred.





AMTD
8, 6355–6393, 2015



Although a significant increase in the number of nucleation mode particles (< 20 nm) was observed during the nucleation phase, these particles were completely evaporated after passing through the TD line at 400 °C.

In the last phase of the experiment, nucleated particles grew up to 100 nm, growing for more than 10 h. After the nucleation event particle number concentration was stabilized and then started decreasing due to wall losses inside the smog chamber. Particles reached a maximum concentration of 6000 $cm^{-3}$ and during aging decreased to 1000 $cm^{-3}$ inside the chamber. The particle number concentration decreased again significantly (NFR = 2 %) after the TD, suggesting that more than 98 % of the particles evaporated at 400 °C. This is an indication that fresh SOA particles produced from the complex ambient organic mixture in a suburban area of Patras evaporate completely after passing through the TD.

Overall, from this set of chamber experiments, the experimental method proposed was able to evaporate almost completely (> 97 %) particles formed from traditional biogenic and anthropogenic SOA precursors and most important, particles coming from a nucleation event.

## 4 Ambient measurements

### 4.1 Instrumentation

During the winter of 2013 (7 January to 5 February) an intensive field campaign was conducted at the premises of the National Observatory of Athens, located in the centre of the city (37°58′21.37″ N, 23°42′59.94″ E). The major objective of this campaign was to determine local and regional air pollution sources in the Greek capital (3.8 million people) during wintertime with a main focus on air pollutants originating from the increasing burning of biomass for residential heating. The measurement site was in the center of Athens, 200 m from the nearest road and is considered an urban background





AMTD
8, 6355–6393, 2015



site. The measurements took place on top of a rocky cliff, opposite of the temple of Thissio.

A suite of instruments was used to characterize the aerosol phase. The TD was coupled with a high resolution time of flight aerosol mass spectrometer (HR-ToF-AMS, Aerodyne), measuring the chemical composition and mass size distribution of $PM_1$ aerosol. A scanning mobility particle sizer (SMPS, TSI) was also connected to the TD providing the number size distribution of the aerosol in the range from 10 to 500 nm. The SMPS was operated with sheath and sample air flows set at 5 and 1 L $min^{-1}$, respectively. To measure the $PM_{2.5}$ black carbon mass concentration a multi-angle absorption photometer (MAAP, model 5012, Thermo-Scientific) was used.

The TD was operating at different temperatures, ranging from 40 to 400 °C (Fig. S1). More specifically, seven temperature steps were chosen for the campaign (40, 70, 100, 120, 200 and 400 °C). One cycle, from 40 to 400 °C and back required 10 h, which resulted in roughly two temperature cycles per day. The starting time of each cycle changed from day to day, to early morning (02:30–05:00 LT), morning (07:00–10:00 LT), afternoon (16:00–18:00 LT) and midnight (21:00–00:00 LT) so that measurements at each temperature were performed during different periods of the day. The temperature of interest for the present work is 400 °C and during the campaign there were 32 periods of measurements at this temperature, resulting in 20 h of data.

AMS analysis and source apportionment of the $PM_1$ organic fraction for the Athens 2013 campaign is given by Florou (2014). Briefly, AMS analysis was performed with the analysis software SQUIRREL v1.51 C and the standard HR-ToF-AMS data analysis software Peak Integration by Key Analysis (PIKA v1.10 C) adapted in Igor Pro 6.22 A (Wavemetrics). Positive matrix factorization (PMF) was applied to the ambient measurements of the AMS organic spectra, following the approach of Ulbrich et al. (2009), to estimate the contributions of the various sources to the organic aerosol (OA) levels.





AMTD
8, 6355–6393, 2015



### 4.2 Chemical characterization of ambient and thermodenuded aerosol

The 32 measurement periods when the TD was set at 400 °C, were analyzed with a focus on number concentration and size distribution of particles with a non volatile core. A summary of the particle number fraction remaining (NFR) after passing through the TD is shown in Fig. 11a. NFR for all the time periods measured, was highly variable, especially during midnight and early morning hours with values ranging from 0.3 to 0.9. The morning NFR ranged from 0.2 to 0.7 while the afternoon values were more stable giving a NFR ranging from 0.3 to 0.5. A correlation of the NFR with BC mass concentration was evident as shown in Fig. 11b. The higher the BC mass concentration the higher the NFR measured. During certain morning periods BC mass concentration reached values $> 3\,\mu g\,m^{-3}$ while the NFR was $< 0.65$. During these periods particles were mostly related to combustion processes due to traffic events and are discussed in detail in Sect. 4.4.

The average mass concentration of the major $PM_1$ species during the time that TD was set at 400 °C combined with the PMF analysis of the organics, for ambient (BP line) and thermodenuded conditions (TD line), are given in Table 3. During ambient measurements, organics dominated the $PM_1$ mass concentration with a 70 % contribution, while black carbon (BC) was responsible for another 17 % (fractions were estimated assuming that BC is found entirely in $PM_1$ scale). The remaining 13 % consisted of sulfate, nitrate and ammonium.

Since organics dominated the total mass, further characterization was performed using PMF analysis. Organics were separated in four categories: hydrocarbon-like OA (HOA) coming from traffic, biomass burning OA (BBOA) due to fireplace and woodstove use for residential heating, oxygenated organic aerosol (OOA) corresponding to long range transport OA, and organic aerosol related to cooking activity (COA). During ambient measurements biomass burning aerosol, contributed 30 % of the organic mass, due to increased burning of wood for domestic heating. BBOA had high levels mostly during the night. A high contribution of aged organic aerosol (28 %) was





AMTD
8, 6355–6393, 2015



observed during low concentration periods. During these periods, mostly rainy days, most of the OA is transported to Athens from other areas. Aerosol emitted by traffic was 25 % of the total organic mass, occurring mostly during the morning and afternoon weekday rush hour traffic. Finally cooking organic aerosol contributed 17 %. These high levels were probably due to the restaurants close to the sampling site.

The aerosol composition changed, when particles passed through the TD. BC dominated the remaining $PM_1$ mass with a contribution of 51 % while organics were responsible for another 45 % (fractions were estimated assuming that BC is found entirely in $PM_1$ and negligible BC evaporation through the TD at 400 °C). The remaining < 5 % consisted mainly of sulfate. The organic mass fraction remaining (MFR) was 20 %, suggesting that part of the organics was of extremely low volatility. Sulfate had a MFR of 10 %, that may be due to larger particles that evaporated partially and entered the detection range of the AMS. The MFR of ammonium and nitrate is subject to a larger relative error since the corresponding concentration values after the TD were close to the detection limit of the instrument.

From PMF analysis, organics after 400 °C were mostly OOA, around 60 %, an expected result, since usually the more oxygenated organic compounds in the aerosol tend to have lower volatility. HOA coming from traffic sources (23 %), biomass burning (13 %) and COA (6 %) were responsible for the rest of the remaining OA.

The increased OOA contribution to the TD organic mass could also be due to oxidation of the organic particles when passing through the TD at 400 °C. This could lead to artifacts in the measurement of the contribution of nonvolatile particles with TD systems. These artifacts could include: (1) pyrolysis of lower volatility organic species at 400 °C potentially leading to an overestimation of the non volatile number and mass concentration; (2) oxidation of BC and non-volatile particles leading to a possible underestimation. These processes have been examined in detail by Novakov and Corrigan (1995). Their work suggested that constituents such as potassium can act as catalysts for the combustion processes and therefore lower the combustion temperature of BC and organics by as much as 100 °C. Applying these to our measurements, for high con-





AMTD
8, 6355–6393, 2015



centrations of potassium (5 % of total mass) we estimated a < 5 % overestimation of the nonvolatile particle mass concentration due to pyrolysis and < 10 % underestimation due to oxidation. These results suggest that although this process might introduce an error in our measurements its contribution is low, increasing our confidence on the resulting non-volatile particle number concentration. Further work is needed in order to explore this process which might constitute a source of error for high temperature TDs.

Given the variability of the measured NFR we focus next on periods when the site was dominated by aerosol from a specific source, to gain insights into the behavior of the corresponding particles. When the fractional source contribution to organic aerosol was higher than 50 % the measurement periods were considered "representative" of the emission source. Two major anthropogenic sources were investigated: (1) biomass burning and (2) traffic.

### 4.3 Biomass burning periods

The correlation between NFR and biomass burning contribution to OA is shown in Fig. 12. As the BBOA fraction increased the NFR increased also ($R^2$ = 0.76). For periods when the BBOA was dominant NFR exceeded 80 %, an indication that most biomass burning particles did not evaporate completely in the TD system at 400 °C. Periods when the BBOA contribution was < 10 % were dominated from aerosol coming from other sources, mostly traffic (Fig. S2).

The particle number size distribution from a major biomass burning period (BBOA was 50 µg m$^{-3}$ and NFR > 90 %) at ambient conditions and at 400 °C is shown in Fig. 13. All the results are corrected for wall losses based on Sect. 2. During this biomass burning event there was a significant shift of the size distribution mode during heating, from 100 to 40 nm, but only a few particles evaporated completely (10 %). This is a strong indication that biomass burning particles have a non-volatile core that survived after 400 °C and were coated with compounds that evaporated through the system and led to a decrease of particle size. Although > 90 % of the particle number concentration was in the size range from 10 to 100 nm the chemical characterization





AMTD
8, 6355–6393, 2015



of these particles was based on the mass concentration, that reflects mainly particles larger than 100 nm. This asymmetry may add uncertainties to this characterization.

During ambient measurements (BP mode) organics dominated the $PM_1$ mass concentration with a 70–75 % contribution, while black carbon (BC) was responsible for another 20 %. The remaining 5–10 % consisted of sulfate, nitrate, and ammonium. The aerosol composition changed, when particles passed through the TD. BC dominated the $PM_1$ mass, with a contribution of 60 %, while organics were responsible for another 35–40 %. The remaining < 5 % consisted mainly of sulfate. The MFR of sulfate was 25 % after 400 °C possibly coming from larger particles that evaporated entering the measurement range of AMS. The organic mass fraction remaining is 17 % suggesting that roughly 80 % of the organics evaporated through the TD. Detailed results are given in Supplement Table S2.

The PMF analysis results for the four biomass burning events were averaged, for ambient measurements (BP mode) and after 400 °C (TD mode). BBOA was dominant in the BP and TD measurements with a 75 and 50 % contribution to the organic mass, respectively. HOA and OOA mass fractions remaining were the highest with 33 and 75 %, respectively, suggesting that although BBOA particles dominate in the TD mass, HOA and OOA are the hardest to evaporate completely while 97 % of the COA mass evaporated in the TD. Detailed results are given in Supplement Table S1.

The volatility of the organics that survived the intense heating was estimated using the TD model of Riipinen et al. (2010). Using the average size of particles, $D_p$ = 200 nm, the organic saturation mass concentration was estimated to be less than $10^{-5}$ µg m$^{-3}$ at 298 K, categorizing these organics as extremely low volatility OA (ELV-OA) (Murphy et al., 2014).

### 4.4 Traffic periods

The particle number size distribution from the most dominant traffic period (HOA was 60 % of the OA) at ambient conditions and at 400 °C is shown in Fig. 14. During this





AMTD
8, 6355–6393, 2015



period the ambient particle number size distribution had a peak at 45 nm. After heating at 400 °C the distribution was separated in two, one with a peak at 20 nm and one with a 70 nm peak. The NFR of 60 % indicated that 40 % of the particles evaporated completely in the TD, while the remaining 60 % had a non-volatile core.

During the three representative traffic events when the HOA contribution was higher than 50 % BC dominated the ambient $PM_1$ mass concentration with a 50 % contribution, while organics were responsible for another 35 %. The remaining 10–15 % consisted of sulfate, nitrate and ammonium. The aerosol composition changed, when particles passed through the TD. The BC contribution increased to 80 %, while organics were responsible for another 17 %. The remaining < 5 % consisted mainly of sulfate. The MFR of sulfate was 18 % at 400 °C, possibly coming from larger particles that evaporated partially entering the measurement range of our instruments. The organic MFR was around 25 %, suggesting that a quarter of the organic mass had extremely low volatility. Detailed results are given in Supplement Table S4.

An average of the PMF analysis from the three traffic events was derived for ambient measurements (BP mode) and after 400 °C (TD mode). HOA contributed 70 % of the ambient OA. After passing through the TD, HOA and OOA were the dominant components remaining with a contribution of 55 and 40 %, respectively. BBOA and COA evaporated almost completely with < 5 % contribution to the organic mass. These organics, were again categorized as ELV–OA with a saturation mass concentration estimated to be less than $10^{-5}$ µg m$^{-3}$. Detailed results are given in Supplement Table S3.

## 5 Conclusions

Non-volatile particle number concentration and size distribution were measured using a thermodenuder (TD) operating at 400 °C. The TD is based on the design of An et al. (2007), providing high residence times for the aerosol. The TD maximum temperature was set at 400 °C. The TD setup was coupled with a HR-ToF-AMS, measuring





AMTD
8, 6355–6393, 2015



the chemical composition and mass size distribution of the $PM_1$ aerosol and a SMPS that provided the number size distribution of the aerosol in the range from 10 to 500 nm.

The ability of this system to measure non-volatile particle number distributions was evaluated with a set of smog chamber experiments. It achieved almost complete evaporation (> 98 %) of biogenic and anthropogenic secondary organic aerosol derived from ozonolysis of a-pinene and OH photoxidation of toluene, respectively. In a different test introduction of ambient air in the chamber and exposure to OH radicals induced an ambient nucleation event. The TD was able to fully (99 %) evaporate all the particles coming from the nucleation event as well as the fresh ambient SOA that condensed on them after nucleation.

This experimental approach was applied in a winter field campaign in Athens and provided a direct measurement of non-volatile particle levels. During periods in which the contribution of biomass burning sources was dominant (> 60 %) more than 80 % of the particles survived the intensive heating, suggesting that nearly all biomass burning particles had a non-volatile core. The particles that did not evaporate consisted of 60 % BC and the rest was mostly organics. Organics surviving through the TD were mostly BBOA and OOA, contributing 90 % of the organic mass concentration, while 10–15 % was from HOA and COA.

For periods during which traffic contributed the majority of the OA 50–60 % of the particles had a non-volatile core, while the rest 40–50 % evaporated at 400 °C. The remaining particles consisted mostly from BC (80 % of the mass) while organics were responsible for another 15–20 %. Organics were mostly HOA and OOA, with a contribution of > 95 % to the organic mass concentration.

Overall, this methodology can be applied to measure the non-volatile particle number size distribution and provide a chemical characterization of their mass. Assuming that all particles remaining after the TD have a black carbon core, the methodology also provides an indirect way of measuring the upper limit of the BC contribution to the particle number concentration.





AMTD
8, 6355–6393, 2015



**The Supplement related to this article is available online at doi:10.5194/amtd-8-6355-2015-supplement.**

*Acknowledgements.* This work was supported by the ESF-NRSF ARISTEIA grant ROMANDE, the FP7 IDEAS ATMOPACS project and the EPA STAR program (grant RD-83503501).

## References

An, W., Pathak, R., Lee, B., and Pandis, S.: Aerosol volatility measurement using an improved thermodenuder: application to secondary organic aerosol, J. Aerosol Sci., 38, 305–314, 2007. 6358, 6359

Andreae, M. O. and Gelencsér, A.: Black carbon or brown carbon? The nature of light-absorbing carbonaceous aerosols, Atmos. Chem. Phys., 6, 3131–3148, doi:10.5194/acp-6-3131-2006, 2006. 6357

Barmet, P., Dommen, J., DeCarlo, P. F., Tritscher, T., Praplan, A. P., Platt, S. M., Prévôt, A. S. H., Donahue, N. M., and Baltensperger, U.: OH clock determination by proton transfer reaction mass spectrometry at an environmental chamber, Atmos. Meas. Tech., 5, 647–656, doi:10.5194/amt-5-647-2012, 2012. 6364

Bohn, B., Rohrer, F., Brauers, T., and Wahner, A.: Actinometric measurements of $NO_2$ photolysis frequencies in the atmosphere simulation chamber SAPHIR, Atmos. Chem. Phys., 5, 493–503, doi:10.5194/acp-5-493-2005, 2005. 6361

Bond, T., Doherty, S., Fahey, D., Forster, P., Berntsen, T., DeAngelo, B., Flanner, M., Ghan, S., Kärcher, B., Koch, D., Kinne, S., Kondo, Y., Quinn, P. K., Sarofim, M. C., Schultz, M. G., Schultz, M., Venkataraman, C., Zhang, H., Zhang, S., Bellouin, N., Guttikunda, S. K., Hopke, P. K., Jacobson, M. Z., Kaiser, J. W., Klimont, Z., Lohmann, U., Schwarz, J. P., Shindell, D., Storelvmo, T., Warren, S. G., and Zender, C. S.: Bounding the role of black carbon in the climate system: a scientific assessment, J. Geophys. Res.-Atmos., 118, 5380–5552, 2013. 6357

Burtscher, H., Baltensperger, U., Bukowiecki, N., Cohn, P., Hüglin, C., Mohr, M., Matter, U., Nyeki, S., Schmatloch, V., Streit, N., and Weingartner, E.: Separation of volatile and non-volatile aerosol fractions by thermodesorption:Instrumental development and applications, J. Aerosol Sci., 32, 427–442, 2001. 6358, 6360, 6361





AMTD
8, 6355–6393, 2015



Cappa, C. D. and Jimenez, J. L.: Quantitative estimates of the volatility of ambient organic aerosol, Atmos. Chem. Phys., 10, 5409–5424, doi:10.5194/acp-10-5409-2010, 2010. 6358
Cohen, A., Ross Anderson, H., Ostro, B., Pandey, K. D., Krzyzanowski, M., Künzli, N., Gutschmidt, K., Pope, A., Romieu, I., Samet, J., and Smith K.: The global burden of disease due to outdoor air pollution, J. Toxicol. Env. Heal. A, 68, 1301–1307, 2005. 6357
de Gouw, J. and Warneke, C.: Measurements of volatile organic compounds in the earth's atmosphere using proton-transfer-reaction mass spectrometry, Mass Spectrom. Rev., 26, 223–257, 2007. 6361
Dockery, D., Pope, C., Xu, X., Spengler, J., Ware, J., Fay, M., Ferris, B. G., and Speizer, F.: An association between air pollution and mortality in six US cities, New Engl. J. Med., 329, 1753–1759, 1993. 6357
Donaldson, K. and MacNee, W.: Potential mechanisms of adverse pulmonary and cardiovascular effects of particulate air pollution ($PM_{10}$), Int. J. Hyg. Envir. Heal., 203, 411–415, 2001. 6357
Florou, K.: Continuous, real−time measurement of the chemical composition and size distribution of atmospheric particles using aerosol mass spectrometry, Master's thesis, Chemical Engineering Department of the University of Patras, Patras, Greece, 2014. 6366
Kanakidou, M., Seinfeld, J. H., Pandis, S. N., Barnes, I., Dentener, F. J., Facchini, M. C., Van Dingenen, R., Ervens, B., Nenes, A., Nielsen, C. J., Swietlicki, E., Putaud, J. P., Balkanski, Y., Fuzzi, S., Horth, J., Moortgat, G. K., Winterhalter, R., Myhre, C. E. L., Tsigaridis, K., Vignati, E., Stephanou, E. G., and Wilson, J.: Organic aerosol and global climate modelling: a review, Atmos. Chem. Phys., 5, 1053–1123, doi:10.5194/acp-5-1053-2005, 2005. 6357
Kim, H., Barkey, B., and Paulson, S.: Real refractive indices of $\alpha$- and $\beta$-pinene and toluene secondary organic aerosols generated from ozonolysis and photo-oxidation, J. Geophys. Res., 115, D24212, doi:10.1029/2010JD014549, 2010. 6358
Kostenidou, E., Pathak, R., and Pandis, S.: An algorithm for the calculation of secondary organic aerosol density combining AMS and SMPS data, Aerosol Sci. Tech., 41, 1002–1010, 2007. 6362, 6377
Kostenidou, E., Florou, K., Kaltsonoudis, C., Tsiflikiotou, M., Vratolis, S., Eleftheriadis, K., and Pandis, S. N.: Sources and chemical characterization of organic aerosol during the summer in the eastern Mediterranean, Atmos. Chem. Phys. Discuss., 15, 3455–3491, doi:10.5194/acpd-15-3455-2015, 2015. 6364





AMTD
8, 6355–6393, 2015



Kreyling, W. and Scheuch, G.: Clearance of particles deposited in the lungs, Lung Biol. Health Dis., 143, 323–366, 2000. 6357

Künzli, N., Jerrett, M., Mack, W. J., Beckerman, B., LaBree, L., Gilliland, F., Thomas, D., Peters, J., and Hodis, H.: Ambient air pollution and atherosclerosis in Los Angeles, Environ. Health Persp., 113, 201–206, 2005. 6357

Kuwata, M., Kondo, Y., Miyazaki, Y., Komazaki, Y., Kim, J. H., Yum, S. S., Tanimoto, H., and Matsueda, H.: Cloud condensation nuclei activity at Jeju Island, Korea in spring 2005, Atmos. Chem. Phys., 8, 2933–2948, doi:10.5194/acp-8-2933-2008, 2008. 6357

Lee, B. H., Kostenidou, E., Hildebrandt, L., Riipinen, I., Engelhart, G. J., Mohr, C., DeCarlo, P. F., Mihalopoulos, N., Prevot, A. S. H., Baltensperger, U., and Pandis, S. N.: Measurement of the ambient organic aerosol volatility distribution: application during the Finokalia Aerosol Measurement Experiment (FAME-2008), Atmos. Chem. Phys., 10, 12149–12160, doi:10.5194/acp-10-12149-2010, 2010. 6358

Miller, F., Gardner, D., Graham, J., Lee Jr, R., Wilson, W., and Bachmann, J.: Size considerations for establishing a standard for inhalable particles, JAPCA J. Air Waste Ma., 29, 610–615, 1979. 6357

Murphy, B. N., Donahue, N. M., Robinson, A. L., and Pandis, S. N.: A naming convention for atmospheric organic aerosol, Atmos. Chem. Phys., 14, 5825–5839, doi:10.5194/acp-14-5825-2014, 2014. 6370

Novakov, T. and Corrigan, C.: Thermal characterization of biomass smoke particles, Microchim. Acta, 119, 157–166, 1995. 6368

Pathak, R., Stanier, C., Donahue, N., and Pandis, S.: Ozonolysis of $\alpha$-pinene at atmospherically relevant concentrations: temperature dependence of aerosol mass fractions (yields), J. Geophys. Res., 112, D03201, doi:10.1029/2006JD007436, 2007. 6362

Poulain, L., Wu, Z., Petters, M. D., Wex, H., Hallbauer, E., Wehner, B., Massling, A., Kreidenweis, S. M., and Stratmann, F.: Towards closing the gap between hygroscopic growth and CCN activation for secondary organic aerosols – Part 3: Influence of the chemical composition on the hygroscopic properties and volatile fractions of aerosols, Atmos. Chem. Phys., 10, 3775–3785, doi:10.5194/acp-10-3775-2010, 2010. 6358

Riipinen, I., Pierce, J., Donahue, N., and Pandis, S.: Equilibration time scales of organic aerosol inside thermodenuders: evaporation kinetics versus thermodynamics, Atmos. Environ., 44, 597–607, 2010. 6359, 6370





AMTD
8, 6355–6393, 2015



Saleh, R., Khlystov, A., and Shihadeh, A.: Determination of evaporation coefficients of ambient and laboratory-generated semivolatile organic aerosols from phase equilibration kinetics in a thermodenuder, Aerosol Sci. Tech., 46, 22–30, 2012. 6358

Saleh, R., Robinson, E. S., Tkacik, D. S., Ahern, A. T., Liu, S., Aiken, A. C., Sullivan, R. C., Presto, A. A., Dubey, M. K., Yokelson, R. J., Donahue, N. M., and Robinson, A. L.: Brownness of organics in aerosols from biomass burning linked to their black carbon content, Nat. Geosci., 7, 647–650, 2014. 6357

Scheer, V., Kirchner, U., Casati, R., Vogt, R., Wehner, B., Philippin, S., Wiedensohler, A., Hock, N., Schneider, J., Weimer, S., and Borrmann, S.: Composition of semi-volatile particles from diesel exhaust, Tech. rep, SAE Technical Paper, 2005. 6357

Ulbrich, I. M., Canagaratna, M. R., Zhang, Q., Worsnop, D. R., and Jimenez, J. L.: Interpretation of organic components from Positive Matrix Factorization of aerosol mass spectrometric data, Atmos. Chem. Phys., 9, 2891–2918, doi:10.5194/acp-9-2891-2009, 2009. 6366

Wehner, B., Philippin, S., and Wiedensohler, A.: Design and calibration of a thermodenuder with an improved heating unit to measure the size-dependent volatile fraction of aerosol particles, J. Aerosol Sci., 33, 1087–1093, 2002. 6358, 6360

Wehner, B., Philippin, S., Wiedensohler, A., Scheer, V., and Vogt, R.: Variability of non-volatile fractions of atmospheric aerosol particles with traffic influence, Atmos. Environ., 38, 6081–6090, 2004. 6358

Wyler, C., Braun-Fahrländer, C., Künzli, N., Schindler, C., Ackermann-Liebrich, U., Perruchoud, A., Leuenberger, P., Wüthrich, B.: Exposure to motor vehicle traffic and allergic sensitization, Epidemiology, 11, 450–456, 2000. 6357





AMTD
8, 6355–6393, 2015



**Table 1.** Experimental conditions used in $\alpha$-pinene dark ozonolysis and toluene photooxidation experiments.

| $\alpha$-pinene Experiments | Temperature (°C) | RH (%) | Initial $\alpha$-pinene (ppb) | Initial $O_3$ (ppb) | SOA Mass [a] ($\mu g\,m^{-3}$) |
|---|---|---|---|---|---|
| 1 | 25 | 30 | 5.5 | 280 | 3.1 |
| 2 | 25 | 30 | 10 | 300 | 8.7 |

| Toluene Experiments | Temperature (°C) | RH (%) | Initial Toluene (ppb) | Initial $NO_x$ (ppb) | Initial $H_2O_2$ (ppb) | [OH][b] (molecules $cm^{-3}$) | SOA Mass [a] ($\mu g\,m^{-3}$) |
|---|---|---|---|---|---|---|---|
| 1 | 25 | 30 % | 50 | 2 | 2 | $2.4 \times 10^6$ | 1.7 |
| 2 | 25 | 30 % | 50 | 7 | 2.1 | $3.1 \times 10^6$ | 2.2 |

[a] Determined from the SMPS measurements using a density of $1.4\,g\,cm^{-3}$ (Kostenidou et al., 2007).
[b] Initial [OH] after UV lights were turned on, as measured by the decay of toluene.





AMTD
8, 6355–6393, 2015





**Table 2.** Initial species concentration for the induced ambient nucleation experiment.

| Gas Phase | | | | | | |
|---|---|---|---|---|---|---|
| $O_3$ (ppb) | $NO_x$ (ppb) | $H_2O_2$ (ppm) | Isoprene (ppt) | Toluene (ppt) | C8 and C9 aromatics (ppt) | OH[a] (molecules $cm^{-3}$) |
| 34 | 6.4 | 1.34 | 100 | 400 | 900 | $3.7 \times 10^6$ |
| Aerosol Phase | | | | | | |
| AMS | | | | SMPS | | |
| Organics ($\mu g\,m^{-3}$) | Sulfate ($\mu g\,m^{-3}$) | Nitrate ($\mu g\,m^{-3}$) | Ammonium ($\mu g\,m^{-3}$) | Number ($cm^{-3}$) | | Mass[b] ($\mu g\,m^{-3}$) |
| 0.45 | 0.27 | < 0.1 | 0.1 | 400 | | 0.6 |

[a] Average [OH] during the experiment as measured by the decay of n-butanol(d9).
[b] Assumed density of $1.5\,g\,cm^{-3}$.





AMTD
8, 6355–6393, 2015



**Table 3.** Average mass concentration of major species when the TD was set at 400 °C (given for ambient conditions and after 400 °C) during the Athens-2013 campaign.

| Temperature | Organics ($\mu g\,m^{-3}$) | | | | Sulfate ($\mu g\,m^{-3}$) | Nitrate ($\mu g\,m^{-3}$) | Ammonium ($\mu g\,m^{-3}$) | BC ($\mu g\,m^{-3}$) |
|---|---|---|---|---|---|---|---|---|
| Ambient | 10 | | | | 0.74 | 0.55 | 0.36 | 2.5 |
| | [a]BBOA | HOA | OOA | COA | | | | |
| | 31 % | 23 % | 29 % | 17 % | | | | |
| 400 °C | 2.1 | | | | 0.18 | 0.1 | 0.04 | 2.5[b] |
| | BBOA | HOA | OOA | COA | | | | |
| | 13 % | 23 % | 58 % | 6 % | | | | |

[a] Source contribution in (%) for the organic aerosol fraction estimated by PMF analysis.
[b] Assuming zero evaporation of BC at 400 °C.





AMTD
8, 6355–6393, 2015



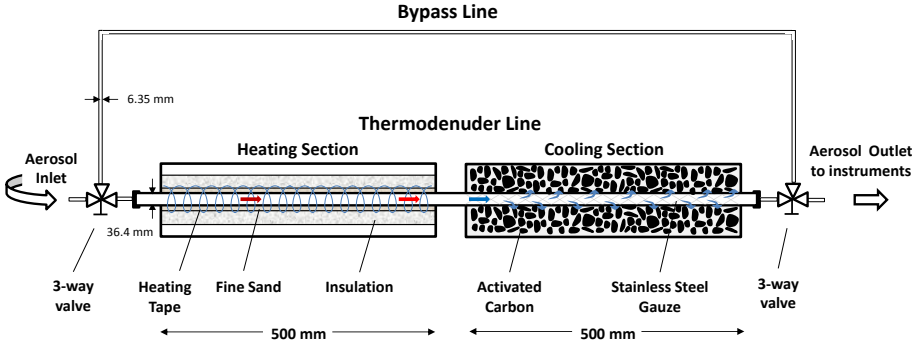


**Figure 1.** Detailed schematic of the thermodenuder used in this study.





AMTD
8, 6355–6393, 2015



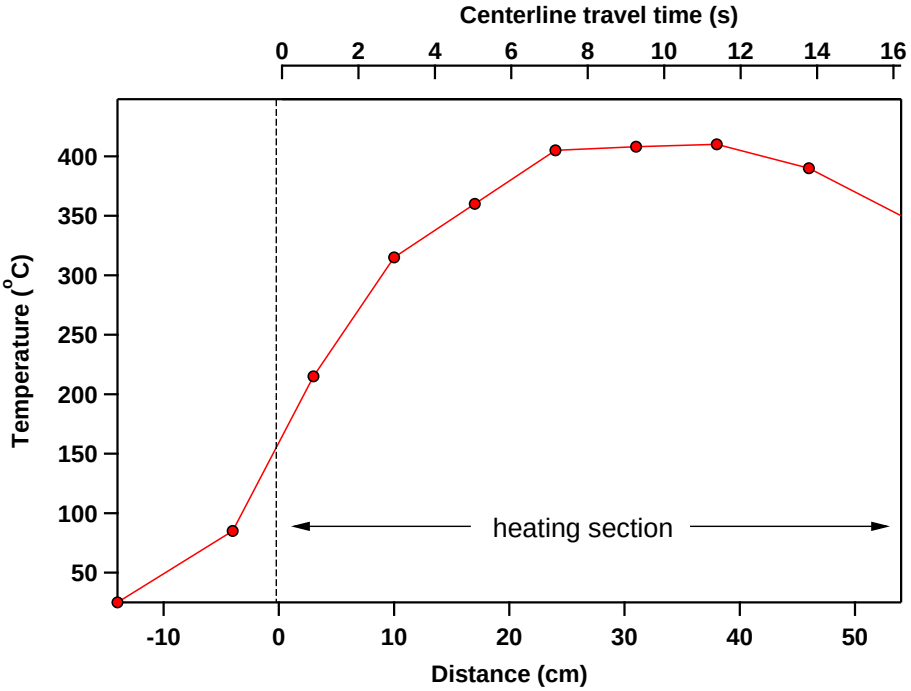


**Figure 2.** Temperature profile inside the heating section of the TD at the set temperature of 400 °C and a flow rate of 1 L min$^{-1}$ as a function of position (distance from the entrance of the heating section, bottom axis) and centerline travel time (top axis).





AMTD
8, 6355–6393, 2015



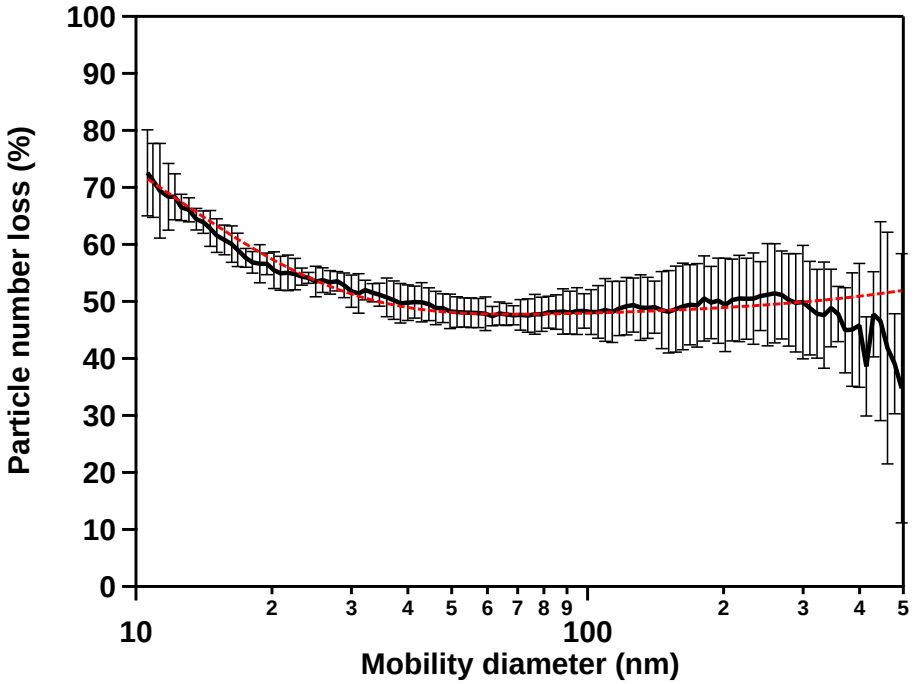


**Figure 3.** Average particle number loss at 400 °C based on 9 different experiments of NaCl aerosol generated with an atomizer, using a flow rate of 1 L min$^{-1}$. The fit function for wall losses is given by the red dash line. The precision ($\pm 2\sigma$) of the average loss correction by the vertical lines. Details are given in the text.





AMTD
8, 6355–6393, 2015



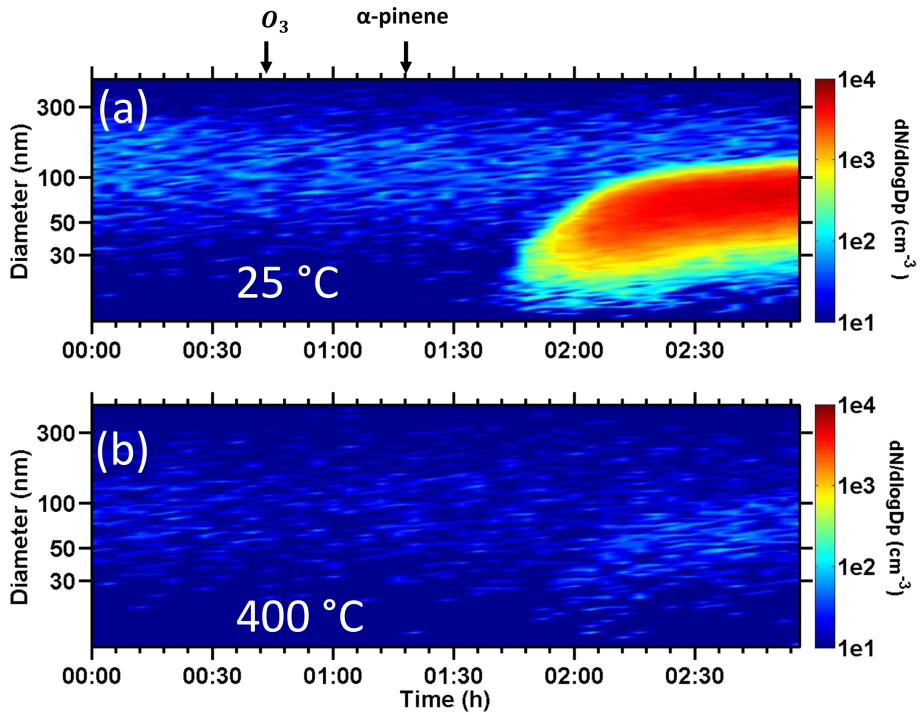


**Figure 4.** Time evolution of particle number size distribution during the dark ozonolysis of $\alpha$-pinene, measured after **(a)** the bypass line at 25˚C and **(b)** the TD set at 400˚C. The color scale represents particle number concentration.





AMTD
8, 6355–6393, 2015



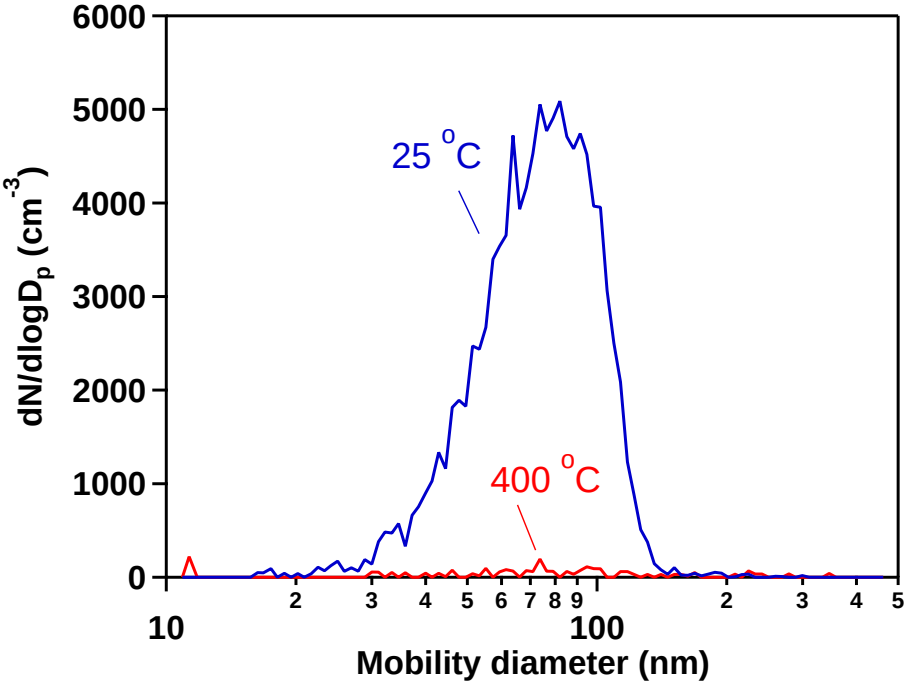


**Figure 5.** Particle number size distribution of $\alpha$-pinene SOA, for chamber measurements, at 25 °C (blue) and loss-corrected TD measurements, at 400 °C (red), for Exp. 1 (see Table 1 for details).





AMTD
8, 6355–6393, 2015



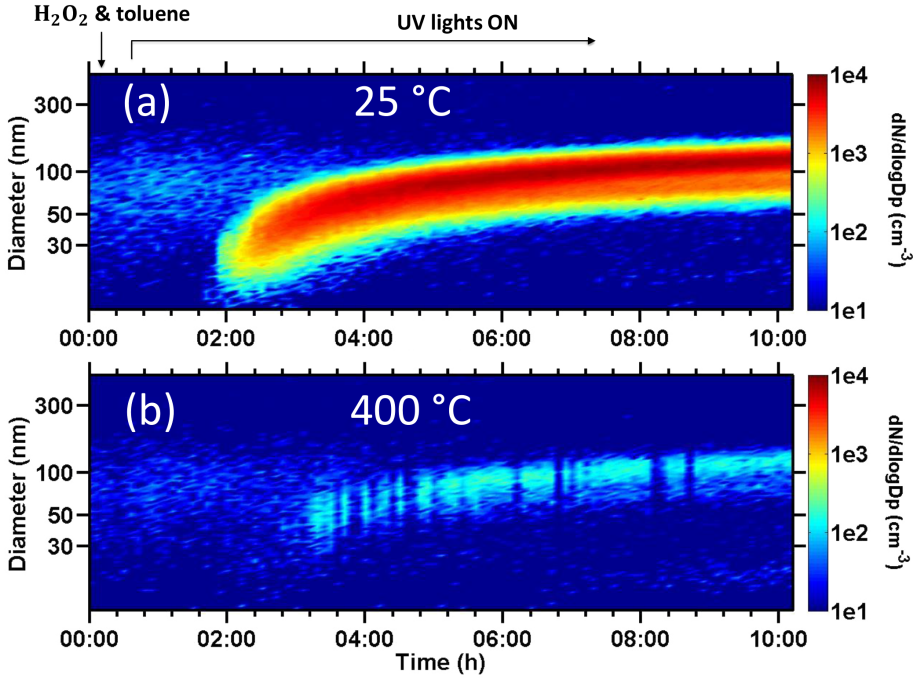


**Figure 6.** Time evolution of particle number size distribution during the photooxidation of toluene, measured after **(a)** the bypass line set at 25 °C and **(b)** the TD set at 400 °C. The color scale represents particle number concentration.





AMTD
8, 6355–6393, 2015



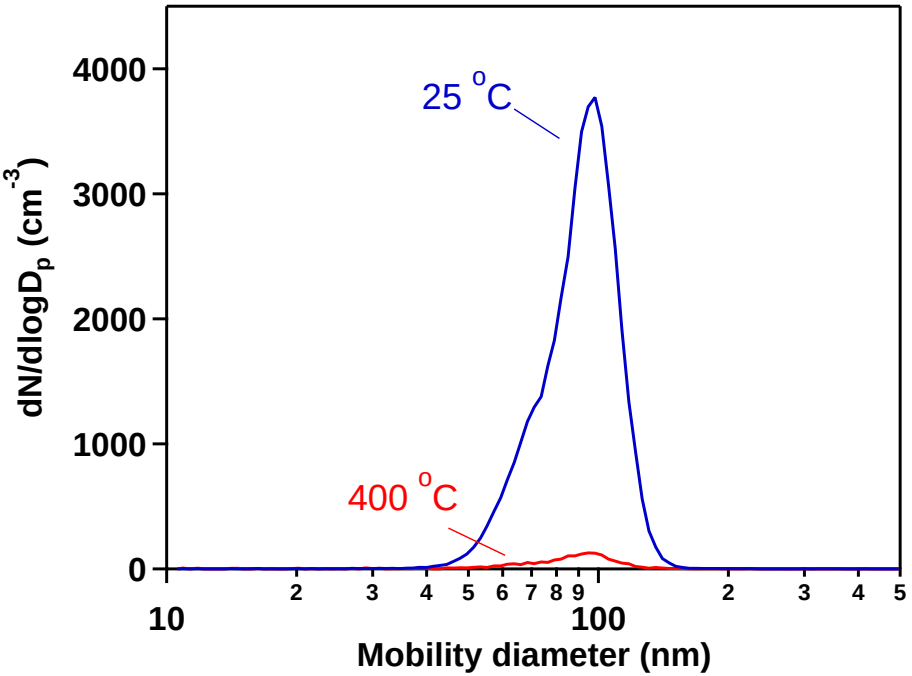


**Figure 7.** Average particle number size distribution (from 07:00 to 09:00) of toluene SOA for chamber measurements, at 25˚C (blue) and TD loss-corrected measurements at 400˚C (red) (Exp. 1, Table 1).





AMTD
8, 6355–6393, 2015



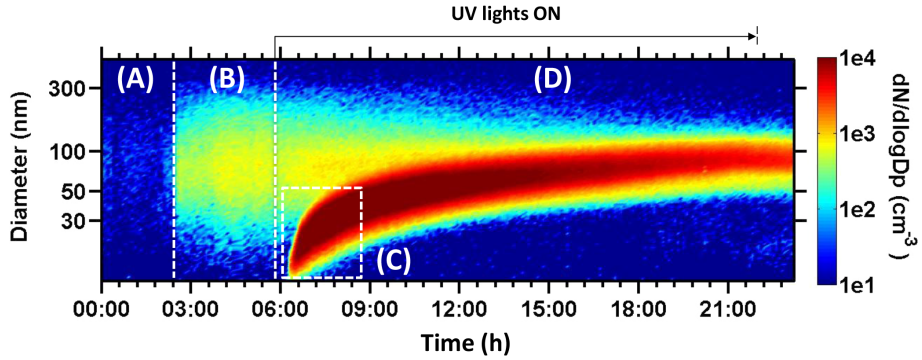


**Figure 8.** Time evolution of particle number size distribution during the induced ambient nucleation experiment, measured after the BP line at 25 ˚C: (A) the chamber background (00:00 to 02:30), (B) introduction of ambient air in the chamber (02:00 to 06:00), (C) nucleation event (06:00 to 09:00) and (D) fresh SOA formation (09:00 to 23:00).





AMTD
8, 6355–6393, 2015



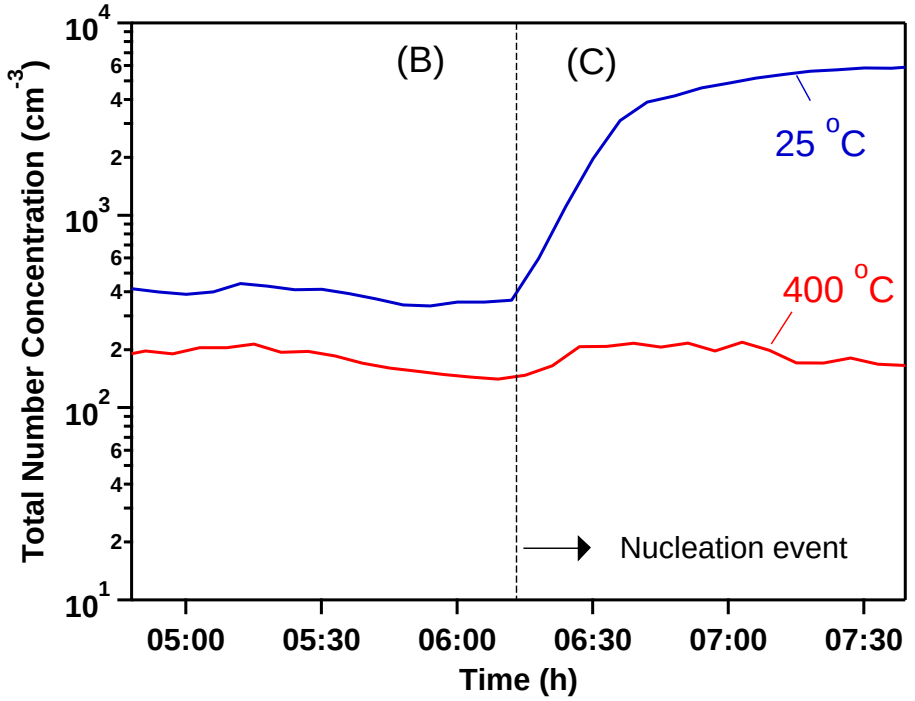


**Figure 9.** Total number concentration of ambient particles introduced in the chamber (Phase B, 04:45 to 06:15) and of particles after nucleation occurs (Phase C, 06:15 to 07:45) as a function of time.





AMTD
8, 6355–6393, 2015



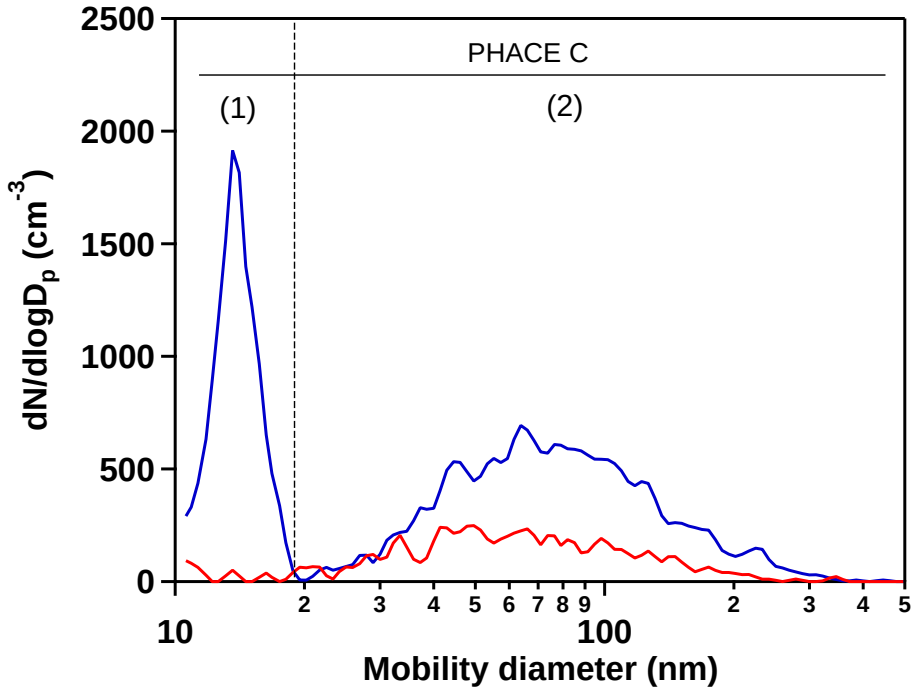


**Figure 10.** The number size distribution during the nucleation event (phase C at 06:15) at 25 ˚C (blue) and 400 ˚C (red). The Aitken mode (2) consists mainly of ambient particles.





AMTD
8, 6355–6393, 2015



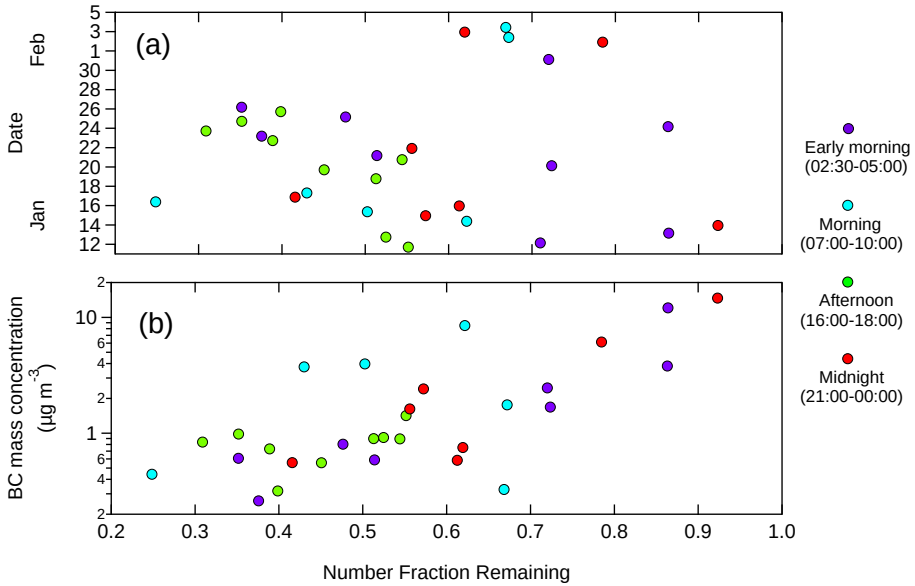


**Figure 11. (a)** NFR during the Athens-2013 campaign when the TD was set at 400°C and **(b)** the correlation of NFR with BC mass concentration measured with MAAP. The different periods of the day are shown with the corresponding colors.





AMTD
8, 6355–6393, 2015



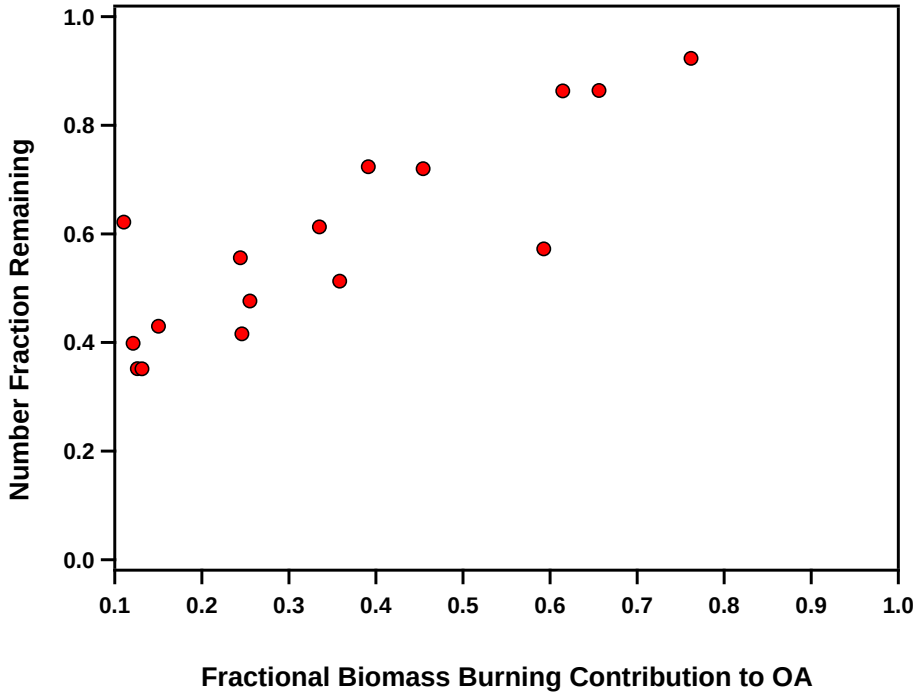


**Figure 12.** The number fraction remaining as a function of the fractional contribution of biomass burning to the organic aerosol mass. Each point corresponds to 0.5–1.2 h.





AMTD
8, 6355–6393, 2015



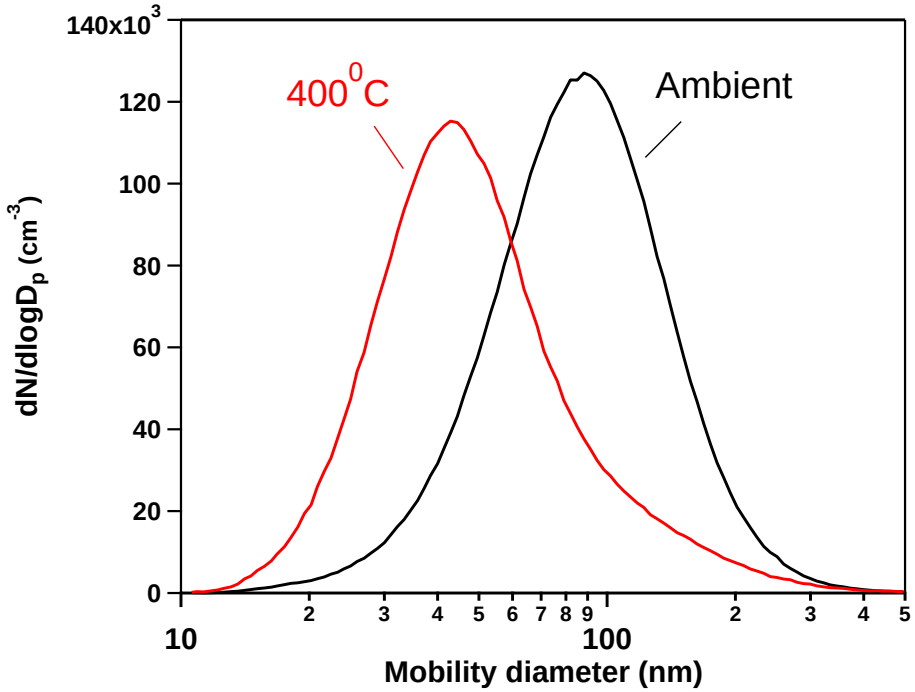


**Figure 13.** Particle number size distribution for a major biomass burning period (BBOA ≃ 75 %) at ambient conditions (black) and 400 °C corrected for losses (red).





AMTD
8, 6355–6393, 2015



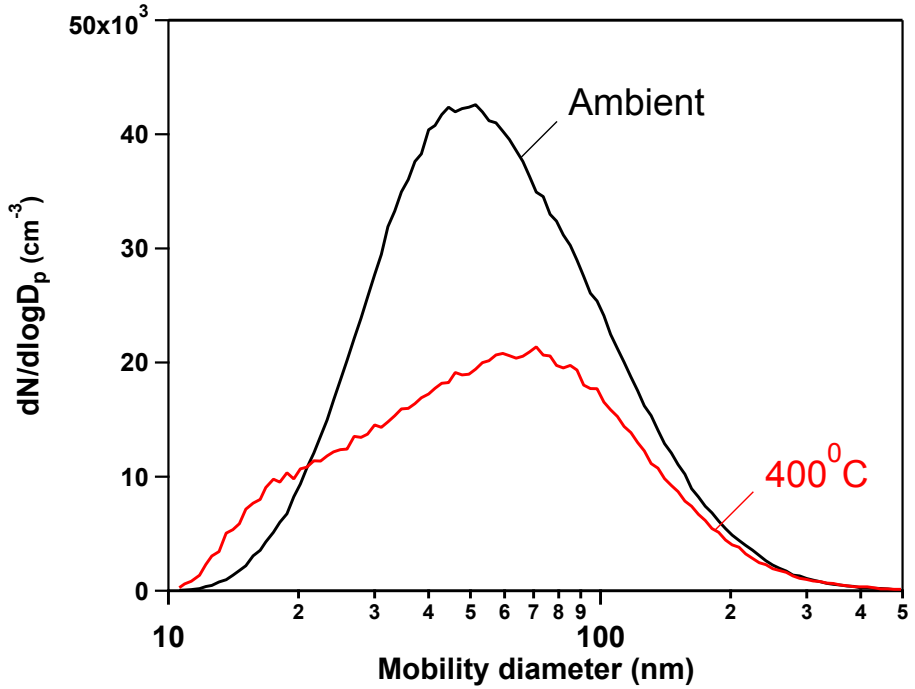


**Figure 14.** Particle number size distribution for a major traffic period (HOA ≃ 70 %), at ambient conditions (black) and 400 °C corrected for losses (red).





AMTD
8, 6355–6393, 2015